Superdirectivity from arrays of strongly coupled meta-atoms

A. Radkovskaya, S. Kiriushechkina, A. Vakulenko, P. Petrov, L. Solymar, L. Li, A. Vallecchi, C. J. Stevens, and E. Shamonina

Citation: Journal of Applied Physics **124**, 104901 (2018); doi: 10.1063/1.5033937

View online: https://doi.org/10.1063/1.5033937

View Table of Contents: http://aip.scitation.org/toc/jap/124/10

Published by the American Institute of Physics

Superdirectivity from arrays of strongly coupled meta-atoms

A. Radkovskaya,[1] S. Kiriushechkina,[1] A. Vakulenko,[1] P. Petrov,[1,a)] L. Solymar,[2] L. Li,[3,b)] A. Vallecchi,[3] C. J. Stevens,[3] and E. Shamonina[3,c)]
[1]*Magnetism Division, Faculty of Physics, M. V. Lomonosov Moscow State University, Leninskie Gory, Moscow 119992, Russia*
[2]*Optical and Semiconductor Devices Group, Electrical and Electronic Engineering (EEE) Department, Imperial College, Exhibition Road, London SW7 2BT, United Kingdom*
[3]*University of Oxford, Department of Engineering Science, Parks Road, Oxford OX1 3PJ, United Kingdom*

(Received 7 April 2018; accepted 5 August 2018; published online 10 September 2018)

We explore the possibility of achieving superdirectivity in metamaterial-inspired endfire antenna arrays relying on the good services of magnetoinductive waves. These are short-wavelength slow waves propagating by virtue of coupling between resonant meta-atoms. Magnetoinductive waves are capable of providing a rapidly varying current distribution on the scale of the free space wavelength. Using dimers and trimers of magnetically coupled split ring resonators with only one element driven by an external source, we introduce an analytical condition for realising superdirective current distributions. Although those current distributions have been known theoretically for a good 60 years, this is the first time that a recipe is given to realise them in practice. Our key parameters are the size of the array, the resonant frequency and quality factor of the elements, and their coupling constant. We compare our analytical results for coupled magnetic dipoles with numerical results from CST simulations for meta-atoms of various shapes. The calculated bandwidth of 5 MHz for a dimer operating at 150 MHz indicates that, contrary to popular belief, superdirective antennas exist not only in theory but may have practical applications. https://doi.org/10.1063/1.5033937

I. INTRODUCTION

Superdirectivity is a topic that reappears at regular intervals in the science and art of electrical engineering starting with the 1922 paper by Oseen[1] in which he refers to "Einsteinian needle radiation." Contrary to phased arrays providing directive radiation by means of constructive interference, superdirectivity is based on the principle that there can be destructive interference in all directions including the direction of the main lobe but that happens to be the direction in which the destructive interference is minimum. The result is somewhat controversial, against common sense. It maintains that arbitrarily high directivity could be achieved with an array of finite size. If this is true, there is no need for enormous apertures: A linear array would do. Let us see an example. At a wavelength of 1 m for a directivity of, say, 10 000, an aperture aerial would require a surface area of about 800 m^2, whereas a superdirective linear array in the endfire configuration could be only a few meters long and have a radial dimension of, say, 10 cm. This is fine in principle. The difficulty is in realisation: how to realise the required current distribution. Apart from the difficulty of producing the right currents, superdirective antennas have of course other limitations: narrow bandwidth, high tolerance sensitivity, and low efficiency are the main ones. For those disadvantages, see, e.g., Ref. 2. In the present paper, we shall concentrate only on the realisation of the required currents for some very limited scenarios. Our primary aim is to maximise directivity without worrying about the necessarily reduced gain and about other limitations. We are interested in applications in which a narrow beam is needed in scenarios when space is limited, e.g., in CubeSats, nanosatellites $10 \times 10 \times 10\,cm^3$ in size.[3] Then what matters is accuracy not power loss or narrow bandwidth.

It has been known for a long time (see, e.g., Ref. 4) that in order to have superdirectivity, the field (or current) should exhibit fast spatial variations. Since most antennas work in free space, the variation has to be fast on the scale of the free space wavelength. To do that is difficult. There have been *ad hoc* solutions (see, e.g., Ref. 5) but no general theory, no general approach. The novel idea in this paper is to use the progress in the theory and practice of metamaterials, in particular that of magnetoinductive (MI) waves,[6,7] to realise the current distribution for 2 and 3-element endfire arrays with elements in the form of split ring resonators.[8,9] In general, MI waves can be employed for guiding and manipulating electromagnetic waves with potential applications ranging from the detection of nuclear magnetic resonance[10,11] to subwavelength imaging[12,13] and wireless power transfer.[14,15] For our purpose, in this paper, what is important is that MI waves are slow waves and consequently have small wavelengths compared to free space signal at equivalent frequencies. Thus, slow change over the wavelength of the magnetoinductive wave means fast change over the free space wavelength and that is exactly what is needed for superdirectivity. Our

[a)]Present address: Department of Physics and Astronomy, University of Exeter, Exeter EX4 4QL, UK
[b)]Present address: Insight Lifetech, Shenzhen 518052, P. R. China.
[c)]Author to whom correspondence should be addressed: ekaterina.shamonina@eng.ox.ac.uk

solution is to realise a superdirective current distribution by launching a magnetoinductive wave. To make that realisation easier and the analogy with magnetoinductive waves even more relevant, we shall restrict our attention to the case when only one of the elements of the array is driven by an applied voltage.

Superdirectivity has a vast literature. A very influential paper was that by Schelkunoff[16] who showed that arbitrarily narrow beams can be obtained with the right design. A rather surprising conclusion was reached by Uzkov[17] who showed that as the length of the linear endfire array tends to zero, the directivity increases as the square of the number of elements in the array. Gain maximisation for a finite number of elements of any linear array was performed by Bloch *et al.*[18] and by Uzsoky and Solymar[19] who also introduced auxiliary conditions defining both an array-Q and tolerance sensitivity. Directivity maximisation for a linear array of dipoles was done by Tai.[20] Generalisation to any dipole distribution (linear, plane, or 3D arrays) was due to Shamonina and Solymar.[21] There were a number of optimisations of Yagi antennas (see, e.g., Refs. 22 and 23) which resulted in much improved directivity but they were still far from superdirectivity. Further progress in the theory of superdirectivity was made by Lo *et al.*[24] who introduced the signal-to-noise ratio as an auxiliary condition when maximising directivity. For some more recent directivity maximisations, see Azevedo[25,26] and Smierzchalski *et al.*[27] The experimental work gained new momentum with the publication of the paper by Newman and Schrote[28] who built a four-element array. More recently, practical superdirective arrays consisting of two elements, driven independently, or parasitic, were reported in Refs. 29–37. The authors stressed the significance of using electrically small resonant elements that eases the problems of impedance matching. Work on metamaterial-inspired superdirective antennas was published in Refs. 38–44.

The aim of this paper is to formulate the design rules for constructing superdirective endfire arrays comprising strongly coupled meta-atoms. The structure of the present paper is as follows. In Sec. II, we treat theoretically the two-element case based on the coupling between resonant elements approximated as magnetic dipoles. "Superdirective conditions" are derived which tells us how two coupled circuits can realise the required superdirective current distribution. The model is tested in Sec. III by comparison to numerical simulations for realistic elements resonant in the MHz frequency range. In Sec. IV, we discuss the issue of the bandwidth, the extension of the model to three-element arrays, and potential applications. Details of analytical derivations are delegated to two Appendixes in order not to interrupt the flow of argument.

II. SUPERDIRECTIVE CONDITIONS FOR A DIPOLE DIMER

A schematic representation of the two-element array is shown in Fig. 1(a). The elements are shown here as split ring resonators[7] widely used for metamaterials, although capacitively loaded rings and squares will also be considered. We shall model the elements arranged in the xy plane at a distance d as two vertical magnetic dipole radiators oriented

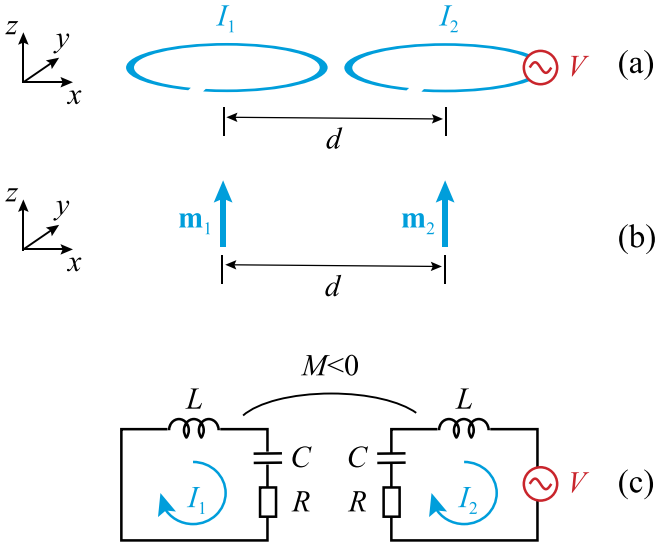

FIG. 1. Schematic representation of a dimer of coupled ring resonators (a), its dipole approximation (b), and coupled LCR model (c).

normally, i.e., along the z axis as shown in Fig. 1(b). The current distribution required for realising superdirectivity is derived in Ref. 21 and given in Appendix A for the general case of N dipole radiators making up a linear array. We shall evaluate them here for the case of two elements and radiation in the endfire (x) direction. The optimum current distribution for two elements presented in the form of a vector with two components I_1 and I_2 has the form

$$\boldsymbol{I}_{\text{opt}} = \boldsymbol{A}^{-1}\boldsymbol{F} = \frac{1}{a^2 - b^2}\begin{pmatrix} a - be^{jkd} \\ ae^{jkd} - b \end{pmatrix}, \tag{1}$$

where

$$\boldsymbol{A} = \begin{pmatrix} a & b \\ b & a \end{pmatrix} \quad \text{and} \quad \boldsymbol{F} = \begin{pmatrix} 1 \\ e^{jkd} \end{pmatrix}, \tag{2}$$

with

$$a = \frac{2}{3}, \quad b = \frac{\sin kd}{kd} + \frac{\cos kd}{(kd)^2} - \frac{\sin kd}{(kd)^3}. \tag{3}$$

$k = \omega/c$ is the wave number, ω is the frequency at which the antenna is radiating, and c is the velocity of light.

We are interested in the $kd \ll 1$ condition when the distance between the elements is small relative to the free space wavelength. We can therefore expand Eq. (1) in terms of kd. We obtain for the ratio of the two currents

$$\left(\frac{I_2}{I_1}\right)_{\text{opt}} = -1 - j\frac{2}{5}kd + \frac{2}{25}(kd)^2 + j\frac{323}{10500}(kd)^3 - \frac{239}{26250}(kd)^4 + \cdots. \tag{4}$$

In the limit of $kd \to 0$, it is sufficient to take into account only the first two terms.

We shall now return to our proposed technique of realising this current distribution. Our goal is to realise the

required current distribution by driving only one of the elements by external voltage and by choosing the right coupling constant and the right quality factors of the two coupled circuits. In this section, we assume that the coupling constant is negative and that element 2 is driven to enable superdirective radiation in the positive x direction. By modelling the meta-atoms as coupled LCR circuits as shown in Fig. 1(c), the ratio of currents for two identical resonant circuits, coupled by a mutual inductance M, is derived in Appendix B as

$$\frac{I_2}{I_1} = -\frac{2}{\kappa}\left(1-\nu^2 - j\frac{\nu}{Q}\right), \tag{5}$$

where

$$Q = \frac{\omega_0 L}{R} \quad \text{and} \quad \kappa = \frac{2M}{L} \tag{6}$$

are the quality factor of the elements and the coupling constant between them, respectively. $\omega_0 = 1/\sqrt{LC}$ is the resonant frequency of the circuit, L is its self-inductance, R the resistance, C the capacitance, and

$$\nu = \frac{\omega_0}{\omega} \tag{7}$$

is the reciprocal frequency of radiation, normalised to the resonant frequency. If we want to realise the superdirective current distribution, the ratio of currents in the coupled circuits should agree with the required current distribution for superdirectivity, i.e.,

$$-\frac{2}{\kappa}\left(1-\nu^2 - j\frac{\nu}{Q}\right) = -1 - j\frac{2}{5}kd. \tag{8}$$

Equating the real and imaginary parts, we find two important conditions

$$\frac{\kappa}{2} = 1-\nu^2 \tag{9}$$

and

$$\frac{|\kappa|Q}{\nu} = \frac{5}{kd}. \tag{10}$$

The first condition [Eq. (9)] may be rewritten as

$$\frac{\omega}{\omega_0} = \frac{1}{\sqrt{1-\kappa/2}} \quad (\text{'SD}_1\text{ condition'}) \tag{11}$$

that unsurprisingly happens to be the same as the resonance frequency of the antisymmetric mode in coupled circuits [Eq. (B9)]. This is very reasonable as superdirectivity for two elements requires the elements to be nearly in antiphase.

The second condition [Eq. (10)] may be rewritten by substituting Eq. (11) into Eq. (10) as

$$\frac{|\kappa|Q}{\sqrt{1-\kappa/2}} = \frac{5}{kd} \quad (\text{'SD}_2\text{ condition'}), \tag{12}$$

which for small coupling constant $\kappa \ll 1$ can be approximated by

$$|\kappa|Q = \frac{5}{kd}. \tag{13}$$

This relationship is valid when the elements are composed of elementary dipoles. For isotropic radiators, the right-hand-side of Eq. (12) modifies to $6/kd$, and, as we will see later, for elements of different shapes, the coefficient on the right hand side will again be different. In this section, we continue considering dipoles but when we come to the CST results, we shall have to modify Eq. (12).

Note that there are five variables ω, ω_0, κ, Q, and d, and there are two equations to satisfy. A possible way to proceed is to choose first the frequency, ω, the coupling constant, κ, and the quality factor, Q, and then find the resonant frequency from Eq. (11) and d from Eq. (12). An alternative is to start with ω and kd because the value of ω is dictated by the system which needs the antenna and d must be chosen so that $kd \ll 1$. Once the physical realisation of the element is chosen, we know the range of values which Q might take. Then, the required coupling constant could be found from Eq. (12).

Equations (11) and (12) have fundamental importance. The first one defines the frequency at which, for a given system of coupled resonators, superdirectivity can occur. The second one is the condition for the existence of superdirectivity, prescribing, for a given geometry (given kd), the required values of the coupling constant κ and the quality factor Q. We shall refer to Eqs. (11) and (12) as the SD_1 and SD_2 conditions. Provided we satisfy SD_2, we have, in the vicinity of the antisymmetric resonance, the current ratio needed for superdirectivity and we can be sure that we have a superdirective radiation pattern. It has been known for a good 60 years what the desired current distribution should be but this is the first time that a recipe has been given how to achieve it. In the present section, the analysis is done for only two elements but this metamaterial-inspired method can also be used for multi-element cases as discussed later.

A superdirective current distribution will yield the maximum achievable for a given frequency and geometry. For a small array with $kd \ll 1$, it is of the form

$$D_{\max} = \frac{21}{4} - \frac{377}{1120}(kd)^2 + \frac{541}{2822400}(kd)^4 \cdots \tag{14}$$

found by expanding Eq. (A10) from Appendix A. Taking just the first two terms of the expansion offers a wide range of validity of up to $kd \simeq 2$ as illustrated by Fig. 2. The maximum as $kd \to 0$ is $D = 5.25$. It is a reasonable value considering that the maximum directivity of an array of N elements is equal to N^2 when $kd \to 0$[17] and the directivity of an elementary dipole (electric or magnetic) is 1.5. (Note here that for finding the resultant radiation pattern, we need to multiply the element radiation pattern with that of the array. This simple method of multiplication does not apply to the respective directivities. The resultant directivity is always less than the product of the individual directivities.)

Let us see now a few examples. In our first example, we intend to show that it is worth adhering to the SD_2 condition and that it will indeed give a superdirective current distribution

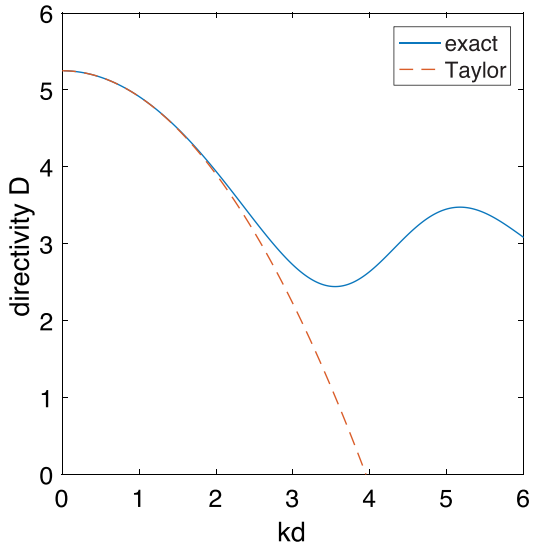

FIG. 2. Optimum directivity for two dipoles vs distance: exact (solid) and Taylor expansion up to the quadratic term (dashed).

and the corresponding high directivity. We shall choose the resonant frequency as $f_0 = 150$ MHz, the inter-element distance as $d = 64$ mm, and the coupling constant as $\kappa = -0.1$. The choice of the coupling constant corresponds to a possible realisation in the form of two closely spaced circular loops, each 62 mm in diameter, in a planar arrangement side by side with the centre-to-centre distance of 64 mm.[45] We shall choose three different values of the quality factor: $Q = 26$ (a), 2600 (b), and 2625 (c) of which the second one satisfies the SD_2 condition and the two others do not, with Q being 10 times smaller than needed in case (a) and 10 times larger than needed in case (c). The modulus of the current ratio, its phase, and the corresponding directivity are shown in Fig. 3 as a function of the normalised frequency for the parameters given above. The maximum directivities obtained in the vicinity of the antisymmetric resonance are 2.28, 5.24, and 4.03 for the three cases, respectively. Insets show the corresponding radiation patterns at the optimum frequency. Although in each of the three cases, the optimum directivity is found in the vicinity of the antisymmetric resonance, i.e., when the SD_1 condition is satisfied, the highest directivity is obtained in case (b), when the SD_2 condition is satisfied as well. The directivity of 5.24 in case (b) does correspond to the theoretical maximum expected for two dipoles with the specified inter-element distance and wavelength, see Eq. (14) and Fig. 2.

Maps of the overall dependence of the optimum directivity for dimer configurations with various values of κ and Q are shown in Fig. 4 as contour plots $D_{max}(\kappa, Q)$ for the parameters: (a) $f_0 = 50$ MHz and $d = 16$ mm, (b) $f_0 = 50$ MHz and $d = 64$ mm, and (c) $f_0 = 150$ MHz and $d = 64$ mm. Every point on each map corresponds to a dimer with specified κ and Q and the frequency yielding the best directivity. The SD_2 condition is also shown as a red dotted line. It may be seen that configurations which satisfy the SD_2 condition for κ and Q indeed show the maximum directivity, whereas for configurations for which the κQ product is too low or too high, the maximum achievable directivity is lower. It is worth mentioning that as long as we keep $kd \ll 1$, the dependence of the optimum directivity on kd is weak, with D gradually reducing from 5.25 at $kd \to 0$ to 5.17 at $kd = 0.5$ [see Eq. (14) and Fig. 2]. Therefore, there will also be very little change in the shape of the optimum radiation pattern for any optimum configuration shown by dashed lines in Fig. 4 in comparison to the radiation pattern already shown in the inset to Fig. 3(b).

It can also be seen from Fig. 4 that, for a sufficiently small coupling constant, the SD_2 condition appears as a straight line on the double logarithmic scale of the graph, yielding evidence that Eq. (13) would be a good

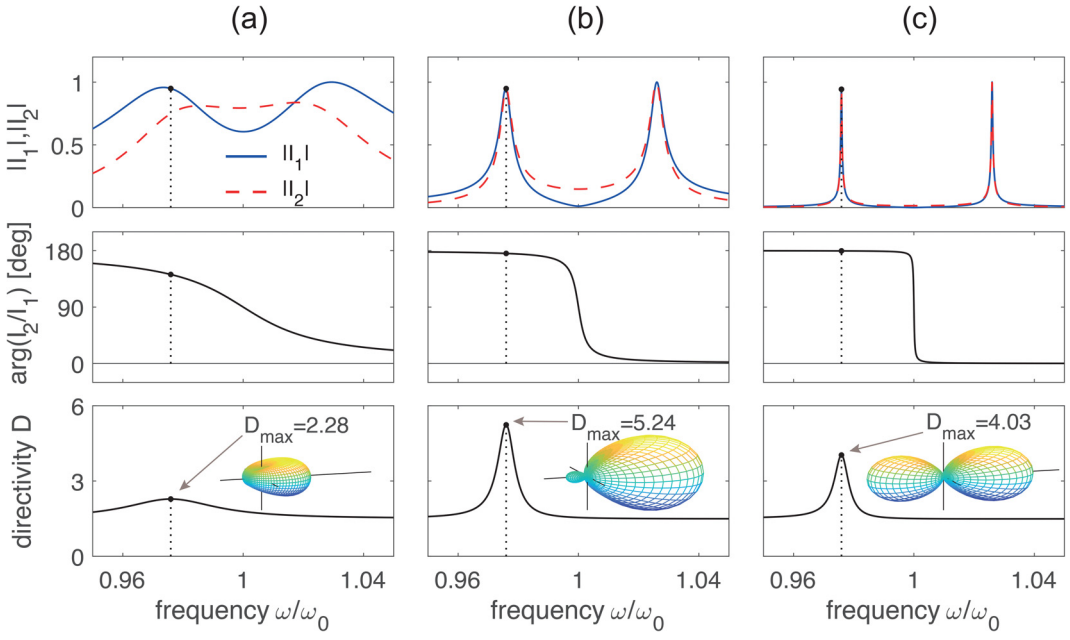

FIG. 3. Frequency variation for the amplitude (top row) and phase (middle row) of dimer's currents and the resulting directivity (bottom row). $f_0 = 150$ MHz, $\kappa = -0.1$, and $d = 64$ mm. Insets show the radiation pattern at the optimum frequency. (a) $Q = 26$; (b) $Q = 262$, and (c) $Q = 2625$.

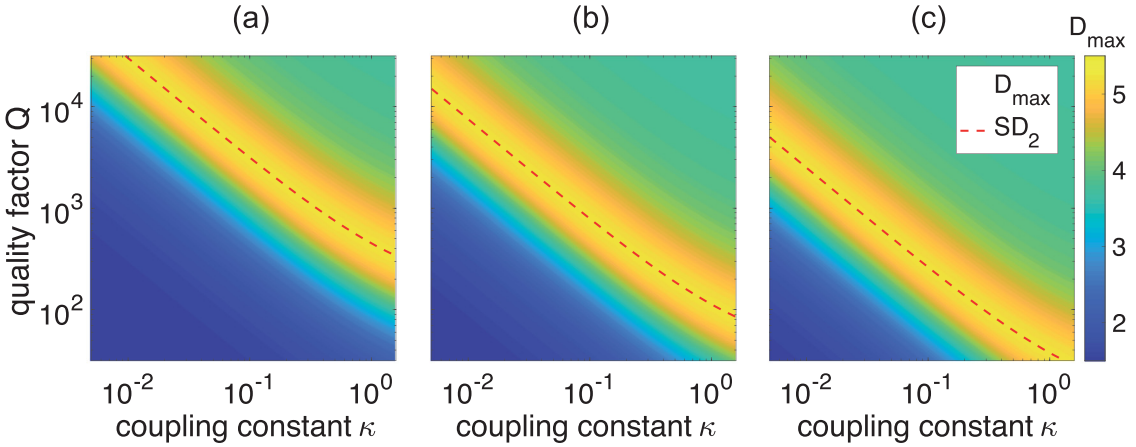

FIG. 4. Maximum directivity D_{max} for a coupled dimer vs. κ and Q (contour plot) and the superdirective condition SD_2 (dashed line). (a) $f_0 = 50$ MHz and $d = 16$ mm; (b) $f_0 = 50$ MHz and $d = 64$ mm, and (c) $f_0 = 150$ MHz and $d = 64$ mm.

approximation of the SD_2 condition. Comparing cases (a)–(c), one can also notice that as kd increases [kd is the smallest in case (a) and the largest in case (c)], the optimum value of the κQ product reduces. This indicates that the choice of κ and Q depends strongly on the size of the array and there might very well be situations when superdirectivity is not achievable, e.g., due to unrealistic values for κ and Q required.

III. SIMULATIONS

To verify our analytical approach enabling us to predict the values of κ and Q that would yield superdirectivity for a chosen geometry, numerical simulations were performed using the time domain solver of CST Microwave Studio. We looked at two types of copper split pipe resonators, of circular and square shape, shown schematically in Fig. 5. To enable a direct comparison between arrays of different shapes, we chose the diameter of circular elements, $2R$, and the side length of the square element, a, both to be equal to 23 mm. Other geometric parameters of the elements were the same for both circular and square elements, namely, the wall thickness $w = 1$ mm, the height $h = 5$ mm, and the gap $g = 2$ mm. By adjusting the value of an external lossless capacitor inserted into the gap of an element, the resonant frequency could be tuned. In the simulations, we excite one of the split pipes by a voltage source and find the current distribution that optimises the directivity by varying the available parameters, namely, the distance between the elements and the resonant frequency.

The capacitively loaded split-pipe elements, although small relative to the wavelength, cannot be regarded simple magnetic dipoles due to their extended height, and hence, we need to generalise the dipole-model SD_2 condition [Eq. (12)] to

$$\frac{\kappa Q}{\sqrt{1-\kappa/2}} = \frac{5\alpha}{kd} \quad (\text{'generalised } SD_2 \text{ condition'}), \qquad (15)$$

where α is a coefficient dependent on the shape of the meta-atom. As mentioned in Sec. II, for isotropic elements, $\alpha = 1.2$, and for dipoles, $\alpha = 1$. We find that for the split pipe elements of extended height $h = 5$ mm used in numerical simulations, for both the circular and square varieties, we need to use $\alpha = 0.8$.

In the first series of simulations, summarised in Fig. 6, we keep the dimer geometry unchanged, with the centre-to-centre distance $d = 24$ mm, i.e., with the separation between

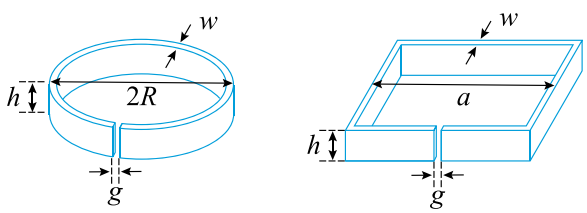

FIG. 5. Circular and square split-pipe elements used in simulations.

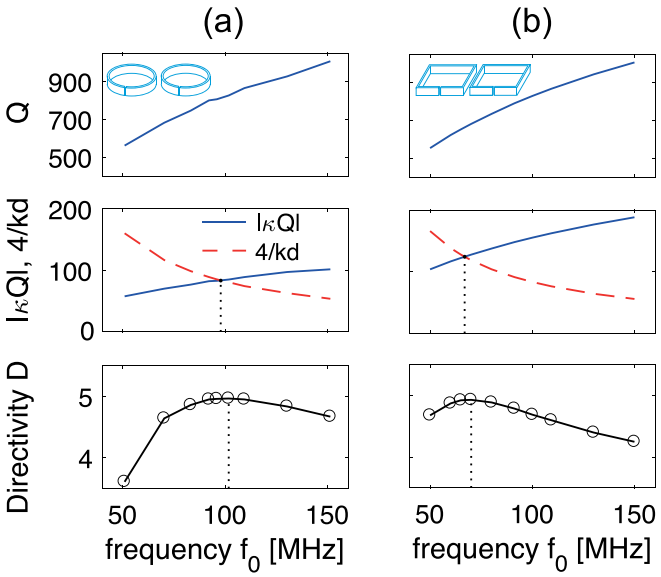

FIG. 6. Verifying superdirective condition SD_2 with simulations. (a) Circular split-pipes with $2R = 23$ mm, $d = 24$ mm, and $\kappa = -0.1$. (b) Square elements with $a = 23$ mm, $d = 24$ mm, and $\kappa = -0.19$. Top row: variation of Q with f_0. Middle row: LHS ($|\kappa|Q$) and RHS ($5\alpha/kd$) of SD_2 with $\alpha = 0.8$. The crossing point of solid and dashed lines indicates the expected optimum resonant frequency. Bottom row: directivity variation with resonant frequency confirms the validity of SD_2 yielding maximum directivity at the expected frequency.

the walls of the neighbouring meta-atoms being 1 mm. The coupling constant for the circular-element dimer for this geometry is found to be equal to $\kappa = -0.1$, and for the square-element dimer, it is -0.19. These values of the coupling constant are calculated from the split of the resonance into the symmetric and the antisymmetric mode, see Eq. (B9), by following the procedure detailed in Ref. 9. By adjusting the value of the capacitors, the resonant frequency varies in the range between 50 and 150 MHz. The left column, Fig. 6(a), shows the results for the circular elements and the right column, (b), is for the square elements. The top row in Fig. 6 shows the numerically calculated variation of the quality factor of a single element with resonant frequency f_0. For elements of either shape, the quality factor increases with the resonant frequency as expected for a copper resonator of the chosen size in the chosen frequency range.

Knowing the numerical values for κ, Q, and kd, we can now employ the generalised SD_2 condition to find the optimum resonant frequency. The middle row of Fig. 6 shows the plots for the frequency dependence of the left-hand side of the generalised SD_2 condition (solid line) and of the right-hand side (dashed line) using the analytical SD_1 condition for the optimum frequency. The numerical data and the analytical data can be seen to agree well. Obviously, the left hand side of SD_2, κQ, increases with increasing frequency because of the increase in Q. The right hand side, $4/kd$, decreases with f_0. Their intersection predicts at what resonant frequency the superdirective condition is fulfilled—this frequency is marked by a vertical dotted line for both types of arrays, for circles (left plot) and for squares (right plot). The optimum frequencies predicted by the SD_2 method are 100 MHz for the circular meta-atoms and 67 MHz for the square meta-atoms.

The bottom row in Fig. 6 shows plots of the directivity values found numerically as a function of the resonant frequency, clearly confirming that the SD_2 condition is indeed valid. Also, in these plots, we mark the optimum frequency by a vertical dotted line, and it can be seen that the values agree well with those predicted by the SD_2 method. The corresponding directivities are close to 5 for both the circular and square elements.

Our next series of simulations (Fig. 7) is analogous to that shown in Fig. 6, but this time, the optimisation is by inter-element distance at a resonant frequency of 150 MHz. The left column (a) is for circular elements and the right column (b) is for square elements. The variation of the coupling constant with the centre-to-centre distance is shown in the top row. As expected, for any distance between the elements, the coupling between square shaped elements is stronger than the coupling between circular elements, because the areas on the two coupled elements are closer to each other. The middle row shows how the left-hand side and the right hand side of the SD_2 condition vary with the centre-to-centre distance. The optimum distance, when the SD_2 condition is fulfilled, is marked by vertical dotted lines for both types of arrays. The directivity plot versus distance in the bottom row demonstrates clearly that our method works again—the maximum directivity corresponds to the predicted distance with good accuracy for both types of arrays. The respective

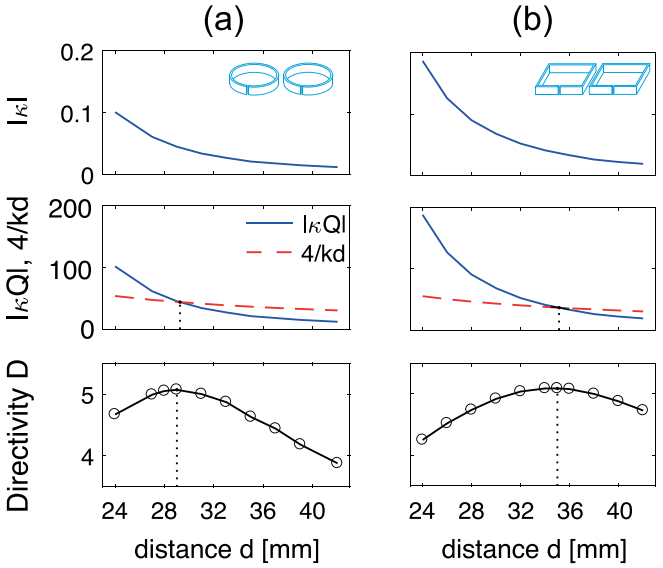

FIG. 7. Verifying superdirective condition SD_2 with simulations. (a) Circular split-pipes with $2R = 23$ mm, $f_0 = 150$ MHz, and $Q = 1000$. (b) Square elements with $a = 23$ mm, $f_0 = 150$ MHz, and $Q = 750$. Top row: variation of $|\kappa|$ with d. Middle row: LHS ($|\kappa|Q$) and RHS ($5\alpha/kd$) of SD_2 with $\alpha = 0.8$. The crossing point of solid and dashed lines indicates the expected optimum centre-to-centre distance between split pipes. Bottom row: directivity variation with the centre-to-centre distance confirms the validity of SD_2 yielding maximum directivity at the expected distance.

optimum directivities are close to 5 in both cases. The optimum centre-to-centre distance for the circular elements is 29 mm, and for the square elements, it is 35 mm. In both cases, when elements are placed side by side, the resulting coupling is too strong, and the elements have to be moved away to reduce the coupling strength to the optimum value, with square elements requiring a larger separation.

Similar optimisation procedures can be performed for other scenarios, e.g., at any resonant frequency. It would not be a difficult exercise to predict that at a lower resonant frequency, as the right hand side of the SD_2 condition is inversely proportional to the frequency (see Fig. 6), a larger value of the coupling constant would be required for the optimum configuration than the values observed in Fig. 7. If the chosen resonant frequency would be too low, the optimisation might fail altogether for the elements of the chosen shape, and a different geometry of meta-atoms would be required that would enhance the coupling constant even further. Suitable candidates would be, e.g., elongated rectangular elements, for which the coupling constant is known to increase significantly.[46]

IV. DISCUSSION

A. Bandwidth

Our SD method provides a simple test whether or not a chosen geometry is capable of superdirectivity. By estimating the product of κQ and comparing it to $5/kd$, we know what changes to the inter-element distance, the resonant frequency, or the shape of the elements are needed for a dimer of meta-atoms to satisfy the SD_2 condition. If, in an optimised configuration, the actual frequency deviates from the optimum one, then of course both the currents and the value

of kd change. As a consequence, both the radiation pattern and the directivity will change, and the radiation pattern will widen and the directivity of the array will decline, as can be seen, e.g., in Fig. 3(b, bottom plot). Our measure of the bandwidth is based upon the decline of directivity. We define the array bandwidth in the usual way

$$\text{array BW} = \Delta f_{3\,\text{dB}}, \tag{16}$$

where $\Delta f_{3\,\text{dB}}$ is the width between the points in frequency where directivity drops by 3 dB from its maximum value obtained at f_{opt}.

How would the configurations shown in Fig. 4 score in terms of the bandwidth? The bandwidth is plotted in Fig. 8 against the absolute value of the coupling constant κ (solid lines) for the parameters corresponding to the optimum SD_2 curve in Fig. 4. We also plot in Fig. 8 the variation of the passband of the corresponding magnetoinductive waves with frequency (dashed lines). The two are obviously correlated although they represent different physical quantities. One shows the frequency range yielding the directivity close to the superdirective value and the other one is the (much wider) frequency range in which magnetoinductive waves can propagate. The fact that both depend on κ in the same manner is a corroboration of our method for realising superdirectivity by virtue of inter-element coupling between meta-atoms.

The bandwidth can be seen to vary between 100 kHz and 5 MHz for realistic values of the coupling constant, $\kappa = -0.1$ to -0.4, for frequencies in the range of 50–150 MHz and distances between the meta-atoms of 16–64 mm. For example, in case (c) with the frequency of 150 MHz, the inter-element distance of 64 mm, and the coupling constant of -0.1, the array bandwidth is 1.6 MHz, and for the coupling constant of -0.4, it is 4.8 MHz. This may be a reasonable value for wireless data transfer applications. Using 64QAM modulation, this would deliver up to 30 Mb/s sufficient for several compressed video channels. Clearly, increasing the frequency or increasing the size of the array, we can increase that number even further. Taking as another example parameters suitable for 700 MHz band UHF TV channel frequencies, choosing $f_0 = 744.5$ MHz, $d = 16$ mm, $\kappa = -0.19$, and $Q = 120$, we obtain the 3 dB bandwidth of over 16 MHz (frequency range 703.2–719.4 MHz), sufficient to cover completely two UHF TV channels, channel 50 and channel 51. Simulation results for split pipes confirm the values of the bandwidth obtained from the dipole model supporting the conclusion that the array bandwidth depends primarily on the coupling strength rather than on the radiation properties of individual resonators.

It can be seen from Fig. 8 that for a larger-size dimer, the bandwidth curve approaches the MI passband curve. Importantly, the values of the bandwidth estimated analytically for dimers agree with those obtained numerically for split-pipe resonators of extended height, suggesting that it is the nature of the magnetoinductive waves and the coupling strength that determine the bandwidth and not so much the actual shape of the resonators. As mentioned before, in a practical realisation, the bandwidth can be increased by making the dimer structure larger by scaling up all the dimensions, while still staying within the requirement of it being small on the scale of the free wavelength. The passband of the magnetoinductive wave sets the asymptotic limit for the bandwidth; hence, realising dimers with a very strong coupling would be the way of achieving a large-bandwidth superdirective performance. Hence, equipped with our simple method of designing superdirective dimers by relying on the SD_2 condition, we can embark on the next stage of optimising superdirectivity by looking at meta-atoms of different shapes while ensuring that the coupling strength is sufficient.

B. Trimers and beyond

Can we find the superdirective condition, analogous to SD_2 for dimers, for a general case of "meta-molecules" comprising many coupled resonators? It would be a worthwhile exercise, considering that the maximum directivity of an array of N elements follows the N^2 trend for $kd \to 0$.[17] The recipe would be the same: by comparing the superdirective current distribution (Appendix A) to that prescribed by the generalised Ohm's law for coupled LCR circuits (Appendix B), we can identify required values of the quality factors and of the coupling constants. How can we match the superdirective current distribution for N elements? The solution is known—the distribution is close to binomial in terms of the amplitude, and the phases are such that the elements are nearly in antiphase. Our intuitive solution is to excite an end-fire array of meta-atoms in the centre, the MI wave that goes in the backward direction from centre to element 1 has to be a backward wave, and hence, the inter-element coupling has

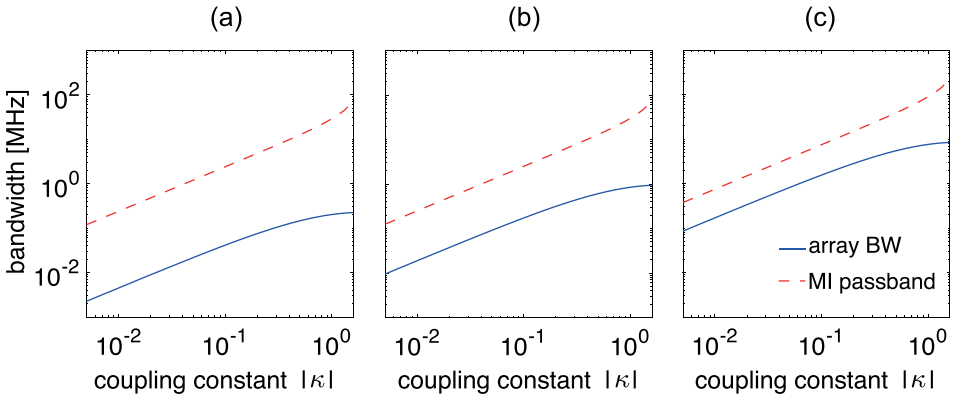

FIG. 8. Array bandwidth for a coupled dimer of dipoles vs. κ at SD_2 condition (solid line) and bandwidth of the MI wave (dashed line). (a) $f_0 = 50$ MHz and $d = 16$ mm; (b) $f_0 = 50$ MHz and $d = 64$ mm, and (c) $f_0 = 150$ MHz and $d = 64$ mm.

to be negative. The other half of the array, from the centre to the end of the array, has to carry a forward wave and that requires positive inter-element coupling. Figure 9 illustrates the principles upon which a superdirective array, realised by magnetoinductive waves, can be built. How can the positive coupling be realised in the planar configuration? One solution would be to use differently shaped elements, e.g., figure-of-eight shaped resonators with an overlap yielding strong positive coupling.[11] Another possibility would be to rely on electric and not magnetic coupling, e.g., by using elements with splits on both sides—that would give positive electric coupling.[47,48]

We test this approach taking a trimer as an example. We return to our analytical dipole model used in Sec. II but consider a trimer, an endfire array of three equidistantly spaced dipoles arranged along the x axis and pointing in the z direction. The optimum directivity of an endfire linear trimer with $kd \ll 1$ can be written as

$$D_{\max} = \frac{735}{68} - \frac{12265}{16184}(kd)^2 - \frac{4658201}{381327408}(kd)^4 + \cdots \quad (17)$$

found by expanding Eq. (A10) from Appendix A. The theoretical value we aim at is a directivity, $D = 10.81$ for $kd \to 0$, a massive improvement in comparison to the two-element directivity, $D = 5.25$. Finding the corresponding expression for the optimum current distribution from Appendix A and expanding it in terms of kd, we obtain

$$\left(\frac{I_1}{I_2}\right)_{\text{opt}} = -\frac{1}{2} + j\frac{17}{168}kd - \frac{5}{84}(kd)^2 + j\frac{16}{1323}(kd)^3 - \frac{11}{3024}(kd)^4 + \cdots, \quad (18)$$

and

$$\left(\frac{I_3}{I_2}\right)_{\text{opt}} = \text{conj}\left(\frac{I_1}{I_2}\right)_{\text{opt}}. \quad (19)$$

As before, in the limit of $kd \to 0$, we shall only take into account the first two terms.

Next, we shall treat the elements of the trimer as coupled LCR circuits and apply the generalised Ohm's law (see Appendix B). We assume for simplicity that only nearest-neighbour coupling matters (hence mutual coupling between elements 1 and 3 is taken as zero, $M_{13} = 0$). Then, the solution for the currents can be written as

$$\left(\frac{I_n}{I_2}\right) = -\frac{\kappa_{n2}}{2}\left(1 - \nu_n^2 - j\frac{\nu_n}{Q_n}\right)^{-1}, \quad n = 1, 3 \quad (20)$$

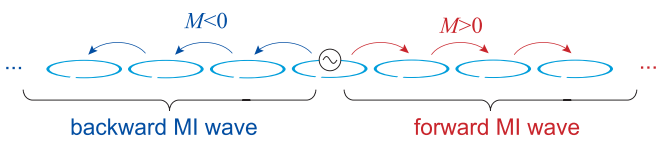

FIG. 9. Schematic of a superdirective array with the central element driven by an external voltage source, with half of the array carrying backward MI waves, and with another half carrying forward MI waves.

with κ_{n2} being the coupling constant between elements n and 2, Q_n is the quality factor of element n, and ν_n is the reciprocal frequency normalised to the resonant frequency ω_{0n} of element n, see also Appendix B. We further assume that although the resonant frequencies in the three elements can be different, $\omega_{01} \neq \omega_{02} \neq \omega_{03}$, their self-inductances and resistances are the same, $L_n = L$ and $R_n = R$ for $n = 1, 2, 3$. The design idea is similar to that of the superdirective dimer case: to have the edge currents almost in anti-phase to the central one, we have to rely on anti-symmetric modes for both the central-left pair and the central-right pair of resonators. To achieve opposite phase shifts for the edge currents $I_1/I_2 = \text{conj}(I_3/I_2)$, we detune the resonances of the edge elements in opposite directions $\omega_{01,03} = \omega_{02}\sqrt{1 \pm \delta}$ and choose the coupling constants between the central element and the edge elements as of opposite sign but equal in magnitude $\kappa_{12} = -\kappa_{32} = -\kappa = -\delta$. This enables our design frequency to be equal to the resonant frequency of the central element, ω_{02}, and to be simultaneously in the vicinity of the lower resonance of the left-central pair of resonators (close to the anti-symmetric mode for the pair of I_1 and I_2 currents) and in the vicinity of the upper resonance of the right-central pair (close to the anti-symmetric mode for the pair of I_2 and I_3 currents). Then, the SD_2 condition for such a trimer takes the form

$$\frac{\kappa Q}{\sqrt{1+\kappa}} = \frac{84}{17kd}, \quad (21)$$

which, for small coupling, practically coincides with the SD_2 condition obtained for the dimers, $\kappa Q = 5/kd$.

Figure 10 shows the frequency variation of the currents [the amplitudes (a) and the phases (b)] and the resulting directivity (c) for the optimum case for the same set of parameters as in Fig. 3, $f_{02} = 150$ MHz, $d = 64$ mm, $\kappa = 0.1$, and $Q_2 = 236$. It can be seen that at ω_{02}, I_1/I_2 and I_3/I_2 are complex conjugates of each other and have both the required magnitude and phase yielding the superdirective radiation pattern. Superdirectivity is indeed achieved at $\omega = \omega_{02}$ with $D = 10.78$ which is the maximum value for the chosen distance between the elements. The inset shows the superdirective radiation pattern at 150 MHz. The array bandwidth is 1.4 MHz, and it would further increase to 2.2 MHz if we would use $\kappa = 0.4$.

So far, we have relied on the ability of slow magnetoinductive waves to produce a rapidly varying current distribution required for superdirectivity. Magnetoinductive waves are of course not unique in this sense; one can rely on plasmon waves,[7] on waves traveling on electric dipole arrays,[49] or on complementary dipole arrays,[50] or indeed on other kinds of slow waves. Applications can include wireless communication, and the bandwidth achievable seems reasonable. Another potential application for superdirective metamaterial-based compact-size antennas could be in 1U CubeSats, nanosatellites where space is limited, e.g., to $10 \times 10 \times 10\,\text{cm}^3$, and enhanced directivity is required.[3] X band superdirective antennas would be sufficiently small and compatible with this kind of size-limited platform although efficiency might be a problem.

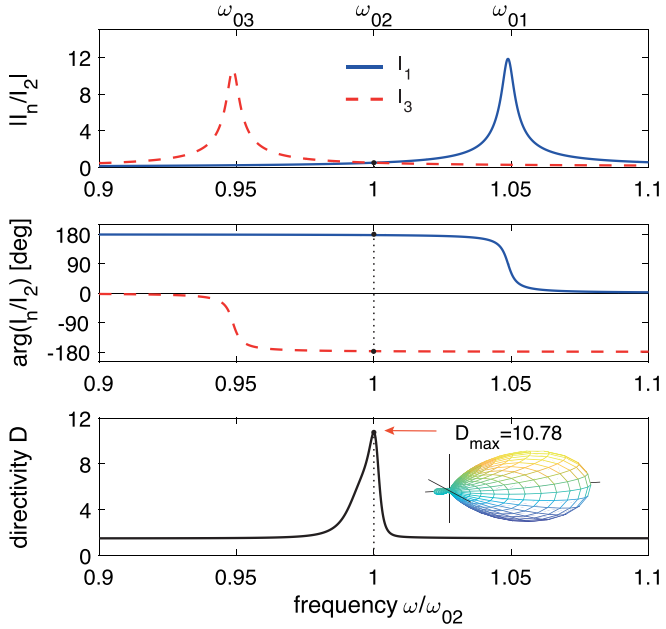

FIG. 10. Superdirective trimer. $d = 64$ mm. Resonant frequencies: $f_{01} = 157.3$ MHz, $f_{02} = 150$ MHz, and $f_{03} = 142.3$ MHz. Quality factors: $Q_1 = 247$, $Q_2 = 236$, and $Q_3 = 223$. Coupling constants: $\kappa_{12} = -\kappa_{31} = -0.1$. Frequency variation for the amplitude (top row) and phase (middle row) of the currents and the resulting directivity (bottom row). The inset shows the radiation pattern at the optimum frequency $\omega = \omega_{02}$.

V. CONCLUSIONS

For the first time to our knowledge, we formulated the design rules for constructing superdirective endfire arrays comprising coupled meta-atoms with only one element being driven by external voltage. The mechanism of imposing the required rapidly varying current distribution is the propagation of slow magnetoinductive waves. Our analytical "superdirective conditions" for the values of the quality factor and the coupling constant allow rapid design of superdirective dimers consisting of two coupled meta-atoms. The analytical model is verified numerically for dimers of capacitively loaded split pipe resonators of circular and square shape. The array bandwidth is shown to be determined by the passband of the magnetoinductive waves and increase with the coupling constant reaching significant values moving superdirectivity from the area of scientific curiosity to the area of practical applications. We conjecture that this model can be generalised to superconductive arrays of $2N + 1$ elements in which the central element is excited and the desired current distribution is obtained by a magnetoinductive forward wave in the direction of endfire radiation and by a magnetoinductive backward wave in the opposite direction.

ACKNOWLEDGMENTS

Financial support by the John Fell Fund (University of Oxford) and by the EPSRC UK (SYMETA, EP/N010493/1) is gratefully acknowledged. We would like to thank also colleagues from the OxiMeta Oxford University Network on Metamaterials for fruitful discussions.

APPENDIX A: SUPERDIRECTIVE LINEAR ENDFIRE ARRAY

The expressions in this Appendix (used in Secs. II and IV) adopt a more general case derived in Ref. 21 for an endfire array of N parallel magnetic dipoles. In the far field, the electric field produced by an N-element array of identical magnetic dipoles placed equidistantly along the x axis pointing in the z direction may be written as the inner product of two N-dimensional vectors $\boldsymbol{I}$ and $\boldsymbol{F}$

$$\boldsymbol{E} = C\boldsymbol{F}\boldsymbol{I}, \tag{A1}$$

where

$$\boldsymbol{I} = [I_1 \ \ldots \ I_m \ \ldots \ I_N] \tag{A2}$$

is the current distribution within the array,

$$\boldsymbol{F} = \sin\theta\left[1, e^{2ju}, \ldots, e^{(N-1)ju}\right] \tag{A3}$$

gives information about the geometry of the array, C is a constant, and

$$u = kd\sin\theta\cos\varphi, \quad k = 2\pi/\lambda. \tag{A4}$$

θ and φ are the elevation and the azimuthal angle of the spherical coordinate system, with θ measured from the axis of dipoles (z axis) and φ measured in the xy plane from the axis of the array (x axis), d is the distance between the elements, and λ is the free space wavelength. The power density is then of the form

$$P_{\mathrm{d}} = \frac{|E|^2}{2Z_0} = \frac{C^2}{2Z_0}\boldsymbol{I}_{\mathrm{H}}B\boldsymbol{I}, \tag{A5}$$

where $\boldsymbol{B}$, an N-dimensional matrix, is expressed as

$$\boldsymbol{B} = \boldsymbol{F}_{\mathrm{H}} \circ \boldsymbol{F}, \tag{A6}$$

the outer product of the vector $\boldsymbol{F}$ with itself, and the subscript H indicates the Hermitian transpose of the vector. The average power density over the solid angle 4π is given by

$$\langle P\rangle = \boldsymbol{I}_{\mathrm{H}}\boldsymbol{A}\boldsymbol{I}, \tag{A7}$$

where

$$\boldsymbol{A} = \frac{1}{4\pi}\int \boldsymbol{B}\sin\theta d\theta d\varphi \tag{A8}$$

with the diagonal and non-diagonal elements in the form

$$A_{nn} = \frac{2}{3},$$
$$A_{nm} = \frac{\sin(|n-m|kd)}{|n-m|kd} + \frac{\cos(|n-m|kd)}{(|n-m|kd)^2} - \frac{\sin(|n-m|kd)}{(|n-m|kd)^3}. \tag{A9}$$

The directivity is then

$$D = \frac{\boldsymbol{I}_{\mathrm{H}}\boldsymbol{B}\boldsymbol{I}}{\boldsymbol{I}_{\mathrm{H}}\boldsymbol{A}\boldsymbol{I}}, \tag{A10}$$

where the power density in the numerator is taken in the endfire, $\theta = \pi/2$, $\varphi = 0$, direction. The optimum current is given as[19]

$$\boldsymbol{I}_{\text{opt}} = \boldsymbol{A}^{-1}\boldsymbol{F} \tag{A11}$$

and the maximum available directivity is

$$D_{\text{opt}} = \boldsymbol{F}_{\text{H}}\boldsymbol{A}^{-1}\boldsymbol{F}. \tag{A12}$$

APPENDIX B: GENERALISED OHM'S LAW FOR COUPLED CIRCUITS

Consider a linear array of N resonant elements modelled as LCR circuits with an inductance, L_n, capacitance, C_n, and resistance, R_n, coupled by mutual inductances, M_{nm}. The general relationship to satisfy is the generalised Ohm's law

$$\boldsymbol{V} = \boldsymbol{Z}\boldsymbol{I} \tag{B1}$$

for the column vectors of the excitation voltages and the resulting currents

$$\boldsymbol{V} = \begin{pmatrix} V_1 \\ V_2 \\ \cdots \\ V_N \end{pmatrix}, \quad \boldsymbol{I} = \begin{pmatrix} I_1 \\ I_2 \\ \cdots \\ I_N \end{pmatrix}. \tag{B2}$$

The impedance matrix $\boldsymbol{Z}$ contains self-impedances of the elements

$$Z_{nn} = j\omega L_n\left(1 - \nu_n^2 - j\frac{\nu_n}{Q_n}\right) \tag{B3}$$

as the main diagonal terms, where

$$\nu_n = \frac{\omega_{0n}}{\omega}, \quad Q_n = \frac{\omega_{0n}L_n}{R_n}, \quad \omega_{0n} = \frac{1}{\sqrt{L_nC_n}} \tag{B4}$$

are the reciprocal frequency normalised to the resonant frequency ω_{0n}, the quality factor, and the resonant frequency of element n. The non-diagonal elements of the matrix Z are the mutual impedances

$$Z_{mn} = j\omega M_{nm}, \quad m \neq n. \tag{B5}$$

The current vector may be obtained as

$$\boldsymbol{I} = \boldsymbol{Z}^{-1}\boldsymbol{V}. \tag{B6}$$

In the special case of a dimer with identical elements (self-impedance, Z_0, mutual impedance, Z_M, with element 2 being excited by an external voltage and element 1 being passive), the currents I_1 and I_2 can be found as

$$I_1 = -\frac{Z_{\text{M}}}{Z_0^2 - Z_{\text{M}}^2}, \quad I_2 = \frac{Z_0}{Z_0^2 - Z_{\text{M}}^2}. \tag{B7}$$

The resonant frequency will split due to the coupling, so there will be a lower and an upper resonance at the frequencies defined by the condition

$$Z_0^2 - Z_{\text{M}}^2 = 0, \tag{B8}$$

yielding

$$\omega_{01,02} = \frac{1}{\sqrt{1 \pm \frac{\kappa}{2}}}, \tag{B9}$$

where

$$\kappa = \frac{2M}{L} \tag{B10}$$

is the coupling constant widely used in the theory of MI waves.[6,7] Note that if the coupling constant is negative, then the lower resonance is antisymmetric, with the currents in antiphase, whereas the upper resonance is symmetric, with both currents in phase. The symmetric and antisymmetric resonances swap if the sign of the coupling constant changes.

Note that the concept of magnetoinductive waves propagating on a chain of coupled meta-atoms is valid also in this elementary case of two coupled meta-atoms. Within the general MI wave picture,[7] a chain of N meta-atoms supports N distinct eigenmodes of magnetoinductive waves (standing MI waves with sinusoidally varying current along the structure with zero currents at the boundaries, i.e., in elements at sites zero and $N+1$)

$$I_l(n) = \sin\left(\frac{n\pi l}{N+1}\right) \tag{B11}$$

for an element n of an eigenmode l, with l varying from 1 to N and n from 0 to $N+1$. In the special case of just two coupled meta-atoms, the two eigenmodes correspond to the symmetric and antisymmetric resonances of Eq. (B9).

[1] C. W. Oseen, "Die Einsteinsche Nadelstichstrahlung und die Maxwellschen Gleichungen," Ann. Phys. **374**, 202–204 (1922).
[2] C. A. Balanis, *Antenna Theory: Analysis and Design*, 4th ed. (Wiley, New York, 2016).
[3] F. B. Ashraf, T. Alam, M. Cho, N. Misran, and M. T. Islam, "Negative-μ metamaterial-based stacked antenna for 1U CubeSat communication," in *Space Science and Communication for Sustainability* (Springer, Singapore, 2018), pp. 265–273.
[4] L. Solymar, "Maximum gain of a line source antenna if the distribution function is a finite Fourier series," IRE Trans. Antennas Propag. **6**(3), 215–219 (1958).
[5] J. M. Bacon and R. G. Medhurst, "Superdirective aerial array containing only one fed element," Proc. IEEE **116**, 365–372 (1969).
[6] E. Shamonina, V. A. Kalinin, K. H. Ringhofer, and L. Solymar, "Magnetoinductive waves in one, two, and three dimensions," J. Appl. Phys. **92**, 6252–6261 (2002).
[7] L. Solymar and E. Shamonina, *Waves in Metamaterials* (Oxford University Press, Oxford, 2009, 2014).
[8] A. Radkovskaya, M. Shamonin, C. J. Stevens, G. Faulkner, D. J. Edwards, E. Shamonina, and L. Solymar, "Resonant frequencies of a combination of split rings: Experimental, analytical and numerical study," Microwave Opt. Technol. Lett. **46**, 473–476 (2005).
[9] E. Tatartschuk, N. Gneiding, F. Hesmer, A. Radkovskaya, and E. Shamonina, "Mapping inter-element coupling in metamaterials: Scaling down to infrared," J. Appl. Phys. **111**, 094904–1–9 (2012).
[10] L. Solymar, O. Zhuromskyy, O. Sydoruk, E. Shamonina, I. R. Young, and R. R. A. Syms, "Rotational resonance of magnetoinductive waves: Basic concept and application to nuclear magnetic resonance," J. Appl. Phys. **99**, 123908–1–8 (2006).
[11] R. R. A. Syms, E. Kardoulaki, M. Rea, K. Choonee, S. Taylor-Robinson, C. Wadsworth, and I. R. Young, "Magneto-inductive magnetic resonance imaging duodenoscope," PIER Prog. Electromag. Res. **159**, 125–138 (2017).

[12]M. J. Freire and R. Marques, "Planar magnetoinductive lens for three-dimensional subwavelength imaging," Appl. Phys. Lett. **86**, 182505–1–3 (2005).
[13]O. Sydoruk, M. Shamonin, A. Radkovskaya, O. Zhuromskyy, E. Shamonina, R. Trautner, C. J. Stevens, G. Faulkner, D. J. Edwards, and L. Solymar, "A mechanism of subwavelength imaging with bi-layered magnetic metamaterials: Theory and experiment," J. Appl. Phys. **101**, 073903–1–8 (2007).
[14]L. Solymar and E. Shamonina, "Optimal power transfer by coupled resonant coils," in *Proceedings of the 5th International Congress on Advanced Electromagnetic Materials in Microwaves and Optics (Metamaterials 2011)*, Barcelona, Spain, 2011, pp. 18–20.
[15]C. Stevens, "Magnetoinductive waves and wireless power transfer," IEEE Trans. Power Electron. **30**, 6182–6190 (2015).
[16]S. A. Schelkunoff, "A mathematical theory of linear arrays," Bell Syst. Tech. J. **22**(22), 80–107 (1943).
[17]A. I. Uzkov, "An approach to the problem of optimum directive antenna design," C. R. (Dokl.) Acad. Sci. URSS **53**, 35–38 (1946).
[18]A. Bloch, R. G. Medhurst, and S. D. Pool, "A new approach to the design of superdirective aerial arrays," Proc. IEEE **100**, 303–314 (1953).
[19]M. Uzsoky and L. Solymar, "Theory of superdirective linear arrays," Acta Phys., Acad. Hung. Sci. **6**, 185–205 (1956).
[20]C. T. Tai, "The optimum directivity of uniformly spaced broadside array of dipoles," IEEE Trans. Antennas Propag. **12**, 447–454 (1964).
[21]E. Shamonina and L. Solymar, "Maximum directivity of arbitrary dipole arrays," IET Microwave Antennas Propag. **9**, 101–107 (2015).
[22]D. K. Cheng and C. A. Chen, "Optimum spacings for Yagi-Uda arrays," IEEE Trans. Antennas Propag. **21**, 615–623 (1973).
[23]C. A. Chen and D. K. Cheng, "Optimum lengths for Yagi-Uda arrays," IEEE Trans. Antennas Propag. **22**, 8–15 (1975).
[24]Y. T. Lo, S. W. Lee, and Q. H. Lee, "Optimization of directivity and signal-to-noise ratio of an arbitrary antenna array," Proc. IEEE **54**, 1033–1045 (1966).
[25]J. A. R. Azevedo, "Antenna pattern control of planar arrays for long distance communications," Adv. Space Res. **43**, 1603–1610 (2009).
[26]J. A. R. Azevedo, "Synthesis of planar arrays with elements in concentric rings," IEEE Trans. Antennas Propag. **59**, 839–845 (2011).
[27]M. Smierzchalski, K. Mahdjoubi, and A. Sharaiha, "Maximum directivity of azimuthal modes antenna," in *Proceedings of the 7th European Conference on Antennas and Propagation (EuCAP)*, Gothenburg, Sweden, 2013, pp. 2092–2095.
[28]E. H. Newman and M. R. Schrote, "A wide-band electrically small superdirective array," IEEE Trans. Antennas Propag. **30**(6), 1172–1176 (1982).
[29]E. E. Altshuler, T. H. O'Donnell, A. D. Yaghjian, and S. R. Best, "A monopole superdirective array," IEEE Trans. Antennas Propag. **53**, 2653–2661 (2005).
[30]T. H. O'Donnell and A. D. Yaghjian, "Electrically small superdirective arrays using parasitic elements," in *Proceedings IEEE APS International Symposium on Antennas and Propagation (APSURSI)*, Albuquerque, USA, 2006, pp. 3111–3114.
[31]S. Lim and H. Ling, "Design of a closely spaced, folded Yagi antenna," IEEE Antennas Wireless Propag. Lett. **5**, 302–305 (2006).
[32]S. Lim and H. Ling, "Design of electrically small Yagi antenna," Electron. Lett. **43**, 3–4 (2007).
[33]A. D. Yaghjian, T. H. O'Donnell, E. E. Altshuler, and S. R. Best, "Electrically small supergain end-fire arrays," Radio Sci. **43**, RS3002, https://doi.org/10.1029/2007RS003747 (2008).
[34]A. D. Yaghjian, "Increasing the supergain of electrically small antennas using metamaterials," in *Proceedings of 3rd European Conference on Antennas and Propagation (EuCAP)*, Berlin, Germany, 2009, pp. 858–860.
[35]T. H. O'Donnell, A. D. Yaghjian, and E. E. Altshuler, "Behavior of a parasitic supergain two-element array in a dielectric," in *Proceedings of IEEE APS International Symposium on Antennas and Propagation (APSURSI)*, Toronto, Canada, 2010, pp. 1–4.
[36]A. D. Yaghjian and H. R. Stuart, "Increasing the bandwidth of electrically small supergain antennas using low-Q electric dipoles," in *Proceedings of 5th European Conference on Antennas and Propagation (EuCAP)*, Rome, Italy, 2011, pp. 2720–2723.
[37]W. Zhao, A. De, Z. Mei, Y. Zhang, and T. K. Sarkar, "Design of a two-element folded-Yagi antenna with super-directivity," in *Proceedings of IEEE APS International Symposium on Antennas and Propagation (APSURSI)*, Spokane, USA, 2011, pp. 942–944.
[38]K. Buell, H. Mosallaei, and K. Sarabandi, "Metamaterial insulator enabled superdirective array," IEEE Trans. Antennas Propag. **55**(4), 1074–1085 (2007).
[39]B. A. Panchenko, "Metamaterials and superdirectivity of antennas," J. Commun. Technol. Electron. **54**, 286–291 (2009).
[40]P. Sharma, D. Arora, and H. Gupta, "Designing superdirective patch antenna array using metamaterial," Int. J. Eng. Res. Technol. **1**, 1–4 (2012).
[41]T. Kokkinos and A. P. Feresidis, "Electrically small superdirective endfire arrays of metamaterial-inspired low-profile monopoles," IEEE Antennas Wireless Propag. Lett. **11**, 568–571 (2012).
[42]E. Shamonina and L. Solymar, "Superdirectivity by virtue of coupling between meta-atoms," in *IEEE Proceedings of 7th International Congress on Advanced Electromagnetic Materials in Microwaves and Optics (Metamaterials 2013)*, Bordeaux, France, 2013, pp. 97–99.
[43]E. Shamonina and L. Solymar, "Superdirective meta-molecules," in *IEEE Proceedings of 8th International Congress on Advanced Electromagnetic Materials in Microwaves and Optics (Metamaterials 2014)*, Copenhagen, Denmark, 2014, pp. 268–279.
[44]P. Petrov, A. Radkovskaya, C. J. Stevens, and E. Shamonina, "Superdirectivity for coupled dimers of meta-atoms at MHz," in *IEEE Proceedings of 11th International Congress on Engineered Materials Platforms for Novel Wave Phenomena (Metamaterials 2017)*, Marseille, France, 2017, pp. 265–267.
[45]O. Sydoruk, A. Radkovskaya, O. Zhuromskyy, E. Shamonina, M. Shamonin, C. J. Stevens, D. J. Edwards, G. Faulkner, and L. Solymar, "Tailoring the near-field guiding properties of magnetic metamaterials with two resonant elements per unit cell," Phys. Rev. B **73**, 224406–1–12 (2006).
[46]R. R. A. Syms, T. Floume, I. R. Young, L. Solymar, and M. Rea, "Flexible magnetoinductive ring MRI detector: Design for invariant nearest-neighbour coupling," Metamaterials **4**, 1–14 (2010).
[47]A. Radkovskaya, O. Sydoruk, E. Tatartschuk, N. Gneiding, C. Stevens, D. Edwards, and E. Shamonina, "Dimer and polymer metamaterials with alternating electric and magnetic coupling," Phys. Rev. B **84**, 125121–1–6 (2011).
[48]S. V. Kiriushechkina, O. A. Kotel'nikova, and A. A. Radkovskaya, "Peculiarities of propagation of electroinductive waves in magnetic metamaterials," Phys. Wave Phenom. **25**, 101–106 (2017).
[49]S. A. Tretyakov and A. J. Viitanen, "Line of periodically arranged passive dipole scatterers," Electr. Eng. **82**, 353–361 (2000).
[50]A. Ludwig, C. D. Sarris, and G. V. Eleftheriades, "Metascreen-based superdirective antenna in the optical frequency regime," Phys. Rev. Lett. **109**, 223901–1–4 (2012).